ARCHIVES OF MECHANICS
Arch. Mech. **77** (1), 53–66, 2025, DOI: 10.24423/aom.4599

The role of sand filler in enhancing the mechanical properties of polymethylmethacrylate composites

R. WOLNY, T. WICZENBACH, L. PACHOCKI,
K. WILDE, M. RUCKA

Department of Mechanics of Materials and Structures,
Faculty of Civil and Environmental Engineering, Gdańsk University of Technology,
Narutowicza 11/12, 80-233, Gdańsk, Poland, e-mails: radoslaw.wolny@pg.edu.pl,
tomasz.wiczenbach@pg.edu.pl (corresponding author),
lukasz.pachocki@pg.edu.pl, krzysztof.wilde@pg.edu.pl, magdalena.rucka@pg.edu.pl

Polymethylmethacrylate (PMMA) is widely used in biomechanics and civil engineering for its properties. While various fillers have been studied to enhance mechanical properties of PMMA, the impact of sand as a filler has been less explored. This study investigates the effects of varying sand content on the mechanical properties and workability of PMMA-based resin composites, assessing their suitability for biomechanical applications. Specimen types with different sand contents (0%, 26%, 30%, and 52%) were examined through the cone spread test for workability, uniaxial tension tests for mechanical properties, and the finite element analysis (FEA) to simulate material behavior. Results were validated against numerical models to evaluate consistency. Adding sand significantly increased the Young modulus by 108%, 174%, and 286% for sand contents of 26%, 30%, and 52%, respectively, while decreasing the Poisson ratio. However, increased sand content reduced workability, highlighting a trade-off between mechanical strength and ease of handling. Numerical simulations, covering the sand volume ratio from 1% to 52% in 1% increments, showed that predictive accuracy varied: differences were up to 20%, for volume ratio up to 30%, while for contents above 30%, the discrepancies between model predictions and experimental data were below 5%. Incorporating sand into PMMA resin enhances its stiffness and suitability for biomechanical specimen testing. Sand-filled PMMA composites show promise for advanced engineering applications, though further optimization is needed to balance workability and mechanical strength.

Key words: polymethylmethacrylate (PMMA), composite materials, mechanical properties, uniaxial tension test, Digital Image Correlation DIC, numerical modelling.

1. Introduction

Polymethylmethacrylate (PMMA) is widely used in the fields of biomechanics [1], medical [2, 3], civil engineering [4], and electronic research [5, 6]. Its versatility stems from exceptional properties such as transparency, lightness, and resistance to weathering, making it a preferred material for many advanced

engineering and medical applications. Research on the modification of PMMA with nanoparticles opens new avenues for creating composites with enhanced electrical, optical, and mechanical properties, significantly broadening its application in modern technologies [6, 7]. The introduction to the synthesis and applications of PMMA in nanotechnology, biomaterial engineering, and electronics underscores the material's ongoing evolution and increasing significance.

Research on synthetic resin composites filled with sand has highlighted their varied mechanical and thermal properties [8–12]. It has been discovered that these properties can significantly change with the introduction of nano-silica particles and other modifications to the resin composition [5, 13, 14]. Additionally, analyses of the effects of diverse types of resins, hardeners, and diluents on the workability of resin mixtures emphasize their importance for potting processes [16].

In experimental studies related to biomechanics, PMMA resin is frequently chosen for embedding specimens [17–20]. Attaching biological samples directly to the standard clamps of a testing machine is challenging due to their complex geometry and soft structure. Therefore, it is necessary to use a potting compound that adapts to the shape of the specimen and ensures a proper grip in the testing machine. Such a potting material needs to have high stiffness and strength compared to the stiffness and strength of the tissue itself. The diversity of tissue types suitable for biomechanical testing, coupled with the broad spectrum of potential results within even a single tissue category, underscores the necessity for a comprehensive statistical analysis. The variability of the results mandates the use of a substantial number of samples to ensure the reliability of the testing outcomes. Consequently, there is a critical need to refine the potting process for embedding these samples.

In composite material research, the Finite Element Method (FEM) is often utilized [21–23]. This allows for a detailed analysis of stress states within the material structure and the determination of effective mechanical properties. For example, in studies [24, 25], a heterogeneous material was examined, which facilitated the determination of Young's modulus and other characteristics. Such numerical studies always require experimental confirmation to validate the model and to identify reference values to which the model should converge [26, 27]. The test providing the most interpretable results is the uniaxial tensile test, from which Young's modulus and Poisson's ratio can be determined, using modern measurement techniques such as Digital Image Correlation, as seen in [28]. The aim of this study is to investigate the impact of using sand as a filler in a PMMA resin mixture for applications in biomechanics research. The study intends to combine experimental and numerical research to determine how filler affects key mechanical parameters and the workability of the material, which is crucial for embedding samples. A novel aspect of this research is the increase of resin stiff-

ness through the addition of sand, leading to reduced displacements of the resin pot in the testing machine, which could enhance the precision and reliability of biomechanical tests. Additionally, this modification results in a cost-effective use of materials, offering economic benefits alongside technical improvements.

2. Experimental methods

2.1. Material and sample fabrication

Mechanical testing utilized dog-bone shaped specimens, designed in compliance with ASTM D638 [29] (type IV) specifications, as depicted in Fig. 1. These specimens measure 121.5 mm in length with a minimum rectangular cross-section of 6×10 mm^2.

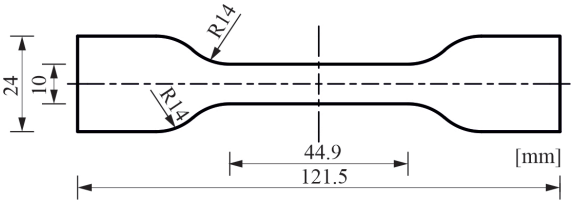

FIG. 1. The geometry of a tensile sample.

The specimens were crafted from PMMA resin (Technovit 3040, Heraeus Kulzer, Wehrheim, Germany [30]). According to the manufacturer's guidelines, the resin should be mixed at a ratio of 2:1, using Technovit 3040 Powder and Technovit Universal Liquid. The specifications for the resin, corresponding to the previously mentioned 2:1 powder to the solvent ratio, are detailed in Table 1.

TABLE 1. Specification of Technovit 3040 resin.

Solidification time [min]	8-10
Density [g/cm^3] (DIN53479)	1.18
Resilience [kJ/m^2] (DIN 13907)	7.1
Bending strength [N/mm^2]	96
Compressive strength [N/mm^2]	110
Young modulus [MPa]	2000–2300

In this study, we created four distinct mixtures, illustrated in Fig. 2: a control mixture using Technovit 3040 Powder (designated as mixture M1) and three additional mixtures incorporating varying amounts of CEN EN 196-1 standard sand [31], labelled as mixtures M2, M3, and M4. For each distinct mixture, we

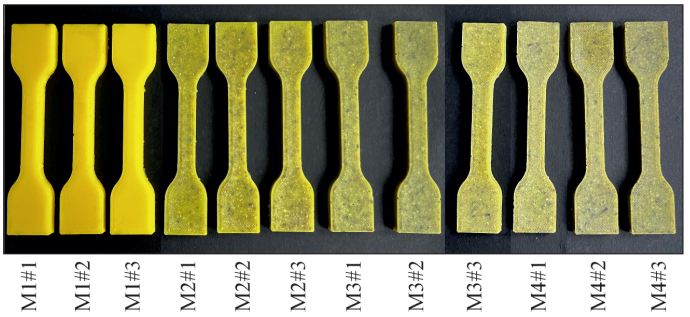

Fig. 2. Overview of tested sample variants: 12 samples across 4 mixture types.

prepared three samples, ensuring a robust data set. Table 2 presents the theoretical composition of these mixtures, showing the quantity of ingredients utilized prior to accounting for any losses during the sample moulding process. The need for a higher ratio of liquid to powder in the mixtures containing sand was to achieve a fluid consistency before the mixtures solidified. The table also indicates the volume ratio of sand and zeolite in the mixture. To counteract sand sedimentation at the bottom, 1g of zeolite was added to each of the sand-containing samples. We also investigated the solidification time of these mixtures, conducting the process in a stable environment with a temperature of 24 degrees Celsius and 37% humidity level. The content percentage was determined by comparing the weight of sand and zeolite to the post-solidification weight of the entire sample. All samples were shaped using silicone moulds.

Table 2. Composition of PMMA samples with varying sand and zeolite contents.

Mixture ID	Powder [g]	Liquid [g]	Sand [g]	Zeolite [g]	Sand and zeolite volume ratio [%]	Samples No.	Avg. density [g/cm^3]
M1	12	6.5	0	0	0	M1#1, M1#2, M1#3	1.08
M2	10	6.5	6	1	$\sim 20\%$	M2#1, M2#2, M2#3	1.35
M3	7	5	11	1	$\sim 36\%$	M3#1, M3#2, M3#3	1.54
M4	5	4.5	16	1	$\sim 52\%$	M4#1, M4#2, M4#3	1.73

2.2. Workability test

The consistency/workability [16] of each mixture type was assessed utilizing a scaled version of the cone method, traditionally employed in laboratories to determine the workability of cement mortars based on mixture flow, in accordance with the PN-EN 13395-1 [32]. A cone with dimensions of 40 mm in bottom diameter, 23 mm in top diameter, and 20 mm in height was used. Following the filling

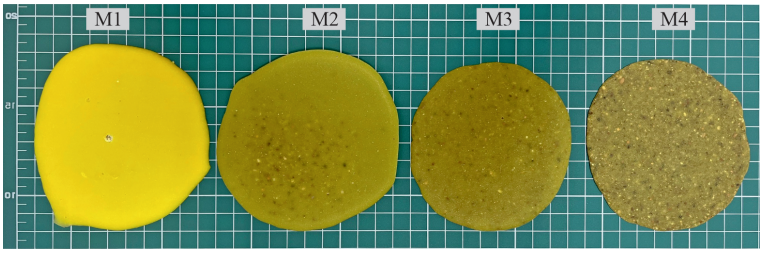

FIG. 3. The spreads after solidification.

of the cone with the mixture, its removal allowed for the measurement of the mixture's spread in two perpendicular directions. The spreads after solidification are depicted in Fig. 3.

2.3. Tensile test

Tensile testing was performed on four distinct sample types, each made from a resin mixture with varying amounts of sand. For each mixture type, three samples were tested using a Zwick/Roell Z10 universal testing machine (Zwick/Roell GmbH & Co. KG, Ulm, Germany). The procedure began with a 10 N preload on the specimen, followed by applying tension at a steady rate of 0.5 mm/min until failure. To assess strains in both horizontal and vertical directions, two virtual extensometers were utilized, as depicted in Fig. 4. Extensometer 1, with a length of 30 mm, recorded vertical deformations, whereas extensometer 2, measuring 8 mm in length, tracked horizontal deformations.

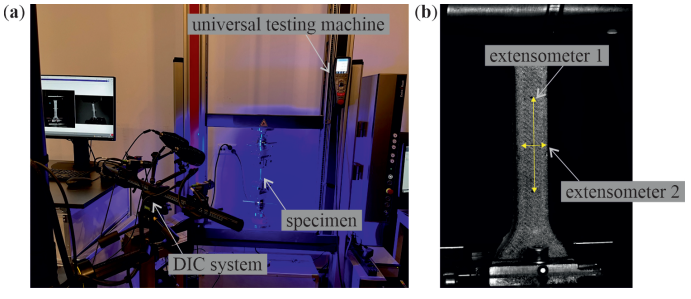

FIG. 4. Experimental setup (a) and configuration of extensometers (b).

3. Numerical model

To simulate the mechanical behaviour of samples composed of the epoxy resin and sand mixture, the Finite Element Method (FEM) approach was utilized, employing ABAQUS/CAE software (Dassault Systèmes, version 2023). The sample

geometry, mirroring the base dimensions of 44.9x10x6 mm^3 as shown in Fig. 1, was first generated. Using a Python script, sand particles, modelled as spheres with diameters ranging from 0.5 to 2 mm, were randomly distributed within the resin. This iterative process aimed to reach target volume ratios of sand to resin, spanning from 0% to the maximum filler volume of 52% as defined in Section 2, with increments of 1%, and ensured no particle collisions occurred.

Meshing was performed using a free mesh algorithm, resulting in a final mesh comprising 102,517 nodes and 593,513 linear quadrilateral elements (C3D4 type) with an element size of 0.5 mm. On the interface between sand particles and resin, nodes were shared to ensure seamless integration. Material models, assumed to be linearly elastic, were characterized by the parameters detailed in Table 3. The properties of the resin were derived from the experimental part of this study. The properties of quartz were obtained from Table II of [33], where the Voigt–Reuss–Hill averaging method was applied. To estimate the isotropic properties of the elastic modulus and Poisson's ratio for our numerical model, we averaged the three values listed in that study.

Table 3. Material properties for numerical analysis.

No.	Material	Young's Modulus [GPa]	Averaged Poisson's ratio [–]	Reference
1	Resin	2.8049	0.3831	Current
2	Quartz	98.4367	0.0647	[33]

Boundary conditions reflective of uniaxial tensile tests were then applied, as illustrated in Fig. 5. The value of the prescribed extension was up to $\epsilon_z = 2‰$ in the longitudinal direction. The analysis was carried out under static mechanical conditions for each volume ratio, conducting 3 simulations per ratio to determine the average effective Young modulus E_{eff}, which is defined as follows:

$$E_{\text{eff}} = \frac{\sum_{i=1}^{n} F_i}{A_0 \times \frac{\Delta L}{L_0}}, \tag{3.1}$$

where $\sum_{i=1}^{n} F_i$ is the total force applied along the longitudinal axis at the boundary of the specimen, A_0 denotes the initial cross-sectional area, ΔL is the displacement applied in the longitudinal direction, and L_0 signifies the initial length.

The transverse strain in the y-direction was determined in correspondence with the procedure from the experimental part. The average value for the central section of the specimen was analyzed. This section was offset by 1 mm from each edge, resulting in an initial width of $w_0 = 8$ mm, as illustrated in Fig. 5. The transverse strain was calculated by averaging the differences between the deformed y-coordinates of nodes n_i and m_i, subtracting the initial width w_0,

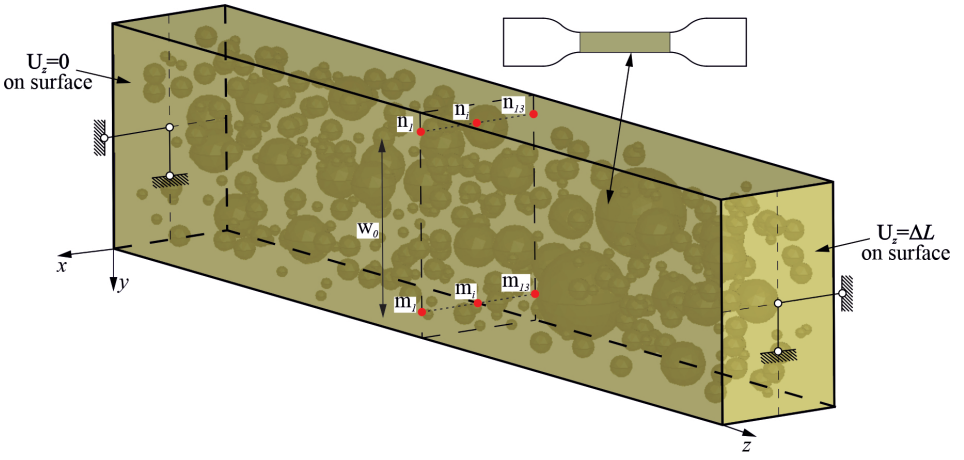

FIG. 5. Scheme of numerical model setup.

and finally dividing by w_0. The formula is expressed as:

$$\epsilon_y = \frac{\frac{1}{13}\sum_{i=1}^{13}(m_i - n_i) - w_0}{w_0}. \tag{3.2}$$

The Poisson ratio was calculated as:

$$\nu = -\frac{\epsilon_y}{\epsilon_z}. \tag{3.3}$$

4. Results

4.1. Solidification time and workability

Table 4 presents the average solidification times across different sand concentrations in the samples. There was a strong correlation (with Pearson's correlation coefficient of 0.72) between the amount of sand and the time it took for the samples to fully solidify. This trend suggests that as the sand proportion in the mixture rises, so does the time required for the sample to completely

TABLE 4. Solidification time of analysed mixtures.

Mixture ID	Solidification time
M1	6 min 57 s ± 29 s
M2	7 min 15 s ± 19 s
M3	7 min 16 s ± 12 s
M4	9 min 36 s ± 20 s

harden. However, for the samples analysed in this study, there was also an increase in the liquid-to-powder ratio, which could influence solidification time. Therefore, establishing a direct cause-and-effect relationship between sand content and hardening time necessitates additional research. Workability tests, assessing how the mixture spreads, indicated a decrease in workability as sand content increased. Specifically, for sand contents of 20%, 36%, and 52%, there was the respective decrease in a spread diameter of about 1%, 9%, and 9%, when compared to the spread diameter of the sand-free mixture.

4.2. Tensile test and identification of material parameters

Young's modulus calculations were carried out for stresses between 2 and 10 MPa. The determination of Poisson's ratio involved using a linear function to fit the relationship between transverse and longitudinal strains, identifying the function's slope as Poisson's ratio. For samples containing 20%, 36%, and 52% sand, there was a respective increase in the average Young modulus of 108%, 174%, and 286% compared to the modulus of the sand-free sample. Concurrently, tensile strength decreased by 49%, 50%, and 55% for these sand contents. Poisson's ratio was reduced to 69%, 68%, and 66% of its original value. Table 5 summarizes the average failure strain, failure stress, Young's modulus, and Poisson's ratio, alongside their standard deviations (SD). Figure 6a displays the stress-strain curves for trials in the longitudinal direction, while Figure 6b illustrates these curves in the transverse direction. Figure 7 depicts the patterns of failure observed.

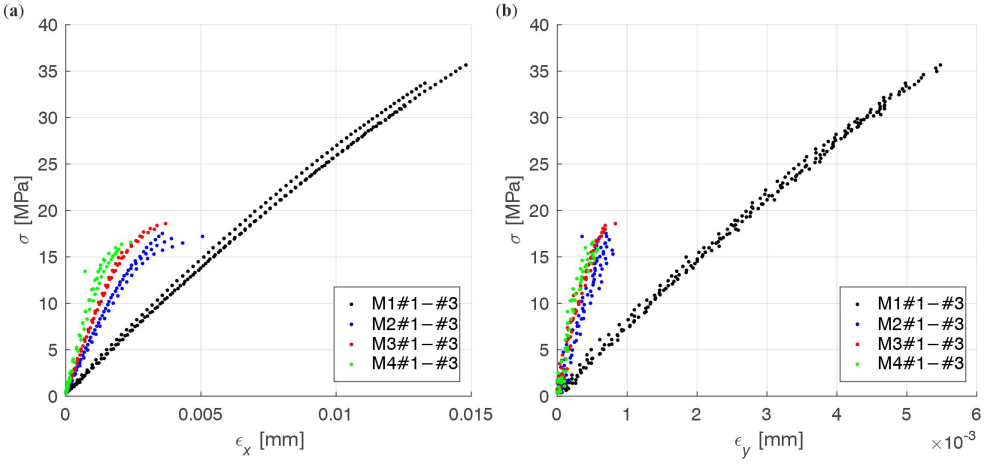

Fig. 6. Stress-strain curves for all samples evaluated: (a) longitudinal strains; (b) transverse strains.

TABLE 5. Mechanical properties of PMMA composites with varying percentages of sand and zeolite.

Mixture ID	Averaged failure strain ± SD [–]	Averaged failure stress ± SD [MPa]	Averaged Young modulus ± SD [GPa]	Averaged Poisson's ratio ± SD [–]
M1	0.0135 ± 0.0011	33.5309 ± 2.2293	2.805 ± 0.0799	0.3831 ± 0.0066
M2	0.0043 ± 0.0007	17.072 ± 0.5291	5.86 ± 0.3096	0.2627 ± 0.0285
M3	0.003 ± 0.0008	17.3402 ± 1.651	7.6794 ± 0.2226	0.262 ± 0.0287
M4	0.0019 ± 0.0005	15.6976 ± 0.9381	10.8139 ± 0.9554	0.2528 ± 0.0198

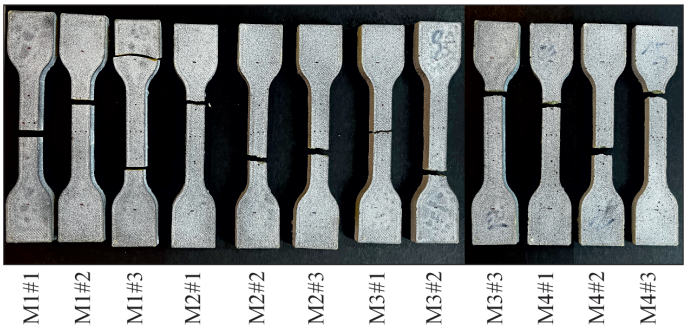

FIG. 7. Failure patterns of all samples.

4.3. FEM results

The FEM model analysis, which incorporated a matrix of randomly placed spherical sand particles, yielded Young's modulus values depicted in Fig. 8. While these values demonstrated a consistent pattern of increased stiffness with added sand, they did not fully align with experimental observations. To quantify

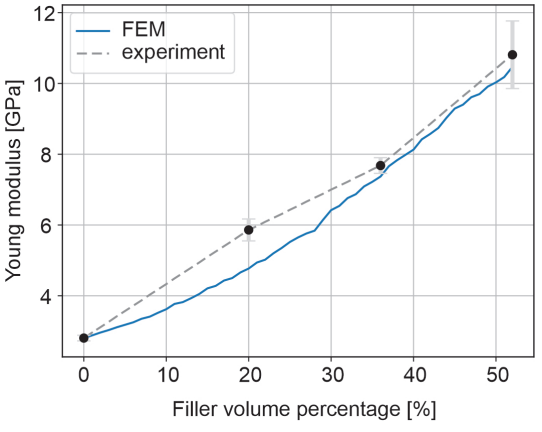

FIG. 8. Comparison of Young modulus results for experiment and FEM.

the relationship between the simulated and experimental data, we linearly interpolated the experimental results and calculated key statistical metrics: the Pearson correlation coefficient (PCC), the Normalized Root Mean Square Error (NRMSE), and the Mean Squared Error (MSE). The values obtained were MSE: 0.41, NRMSE: 0.10, and PCC: 0.99, suggesting a strong linear correlation between the simulation and experimental findings, despite the observed discrepancies in stiffness trends with an increasing sand content.

A comparison of the experimental and numerical Poisson's ratio for specific volume ratios is presented in the Table 6.

Table 6. Experimental and FEM averaged Poisson's ratio ± SD value.

Volume ratio [%]	Experimental Averaged Poisson's ratio ± SD [–]	Numerical Averaged Poisson's ratio ± SD [–]
20	0.2627 ± 0.0285	0.3062 ± 0.0410
36	0.262 ± 0.0287	0.2991± 0.02397
52	0.2528 ± 0.0198	0.2968 ± 0.03744

5. Discussion

This research demonstrated that the chosen ratio of components in the samples yielded a consistency suited for encapsulating biological specimens with complex geometries, a technique that has been effectively applied in biomechanical studies [18]. Increasing the sand content to 52% by volume marginally reduced the mixture's ease of handling by 9%, as per the solvent ratio discussed in the document. Adding sand significantly enhanced the resin's Young's modulus, making the composite stiffer, which is beneficial for mounting biological specimens. Although the tensile strength of the sand-infused resin was lower than that of pure resin, its failure stress remained adequate for supporting biological specimens, such as spinal ligaments. For instance, human spine ligaments can stretch from 1 mm to 13 mm under forces up to 900 N without failing [34–36]. Real-world applications involving the resin-sand composite for spinal ligament tests have validated these observations [18].

The possibility of reducing the powder component in favour of sand, without adversely affecting the material's suitability for biomechanical testing, suggests an area for further investigation. Despite the numerical models and experimental results agreeing on the trend of stiffness increasing with more sand, discrepancies in the precise values of Young's modulus were observed. These variances underscore the challenges and assumptions involved in numerical modelling of composite materials.

Moreover, the study demonstrated the potential of Technovit 3040 resin powder reduction in the preparation of biological material samples for mechanical tests. According to the 2022 price list [30], the cost of sample preparation can be reduced by 48.75%. What is more, the number of samples prepared can be doubled without compromising mechanical properties.

In numerical analysis of composites, simplifications such as perfect adhesion between the resin matrix and sand fillers, or assuming uniformly spherical sand particles, are often necessary to simplify complex simulations. However, real materials seldom exhibit these ideal conditions. Factors such as the bonding quality at the particle-matrix interface, variations in particle size, and the presence of voids or imperfections significantly affect the composite's mechanical properties but are frequently simplified in simulations [37].

Furthermore, representing sand particles as spherical in the finite element method (FEM) models might not capture the true, irregular shapes found in the resin, potentially altering the predicted stress distribution within the composite.

The discrepancy in Young's modulus values between the experimental and simulation results at a 20% volume fraction of sand can be attributed to a non-uniform distribution of sand particles in the experimental specimen. Because liquid PMMA has a lower density than sand particles, the inclusions tend to settle at the bottom during preparation, leading to localized densifications that increase stiffness in those regions – effects that standard modeling assumptions, which presume a random distribution of inclusions, cannot predict. In the experimental setup, virtual extensometers observed the bottom face of the specimen, capturing these localized increases in stiffness. In contrast, the numerical model distributes the inclusions more uniformly throughout the specimen, failing to account for the stiffness variations caused by particle settling.

6. Conclusions

This study has shown that it is both feasible and advantageous to enhance the mechanical properties of PMMA for biomechanical uses by incorporating sand. This modification not only increases the stiffness of the material, making it better suited for embedding biological specimens, but it also offers a more cost-effective and potentially more environmentally friendly alternative to pure PMMA. Although accurately modelling the composite material poses certain challenges, the encouraging agreement between experimental and numerical findings underscores the efficacy of numerical analyses in predicting the behaviour of PMMA-sand composites. Future research should concentrate on optimizing the numerical models to better understand the composite's behaviour and extend its applications in biomechanical engineering.

Declaration of Competing Interest

The authors declare that they have no known competing commercial interests or personal relationships that could have appeared to influence the work reported in this paper.

Acknowledgements

The study was financed by the National Science Centre, Poland, under the project No. UMO-2020/37/B/ST8/03231.

References

1. A. Boger, P. Heini, M. Windolf, E. Schneider, *Adjacent vertebral failure after vertebroplasty: a biomechanical study of low-modulus PMMA cement*, European Spine Journal, **16**, 2118–2125, 2007, https://doi.org/10.1007/s00586-007-0473-0.
2. T. Thielen, S. Maas, A. Zuerbes, D. Waldmann, J. Kelm, *Mechanical material properties of polymethylmethacrylate (PMMA) for medical applications*, Materials Testing, **51**, 203–209, 2009, https://doi.org/10.3139/120.110029.
3. R.Q. Frazer, R.T. Byron, P.B. Osborne, K.P. West, *PMMA: An essential material in medicine and dentistry*, Journal of Long-Term Effects of Medical Implants, **15**, 629–639, 2005, https://doi.org/10.1615/JLongTermEffMedImplants.v15.i6.60.
4. G.O. Martínez-Barrera, O. Gencel, J.M.L. Reis, *Civil engineering applications of polymer composites*, International Journal of Polymer Science, 1–2, 2016, https://doi.org/10.1155/2016/3941504.
5. U. Ali, K.J.Bt. A. Karim, N.A. Buang, *A Review of the properties and applications of poly(methyl methacrylate) (PMMA)*, Polymer Reviews, **55**, 678–705, 2015, https://doi.org/10.1080/15583724.2015.1031377.
6. A. Hazim, H.M. Abduljalil, A. Hashim, *Structural, spectroscopic, electronic and optical properties of novel platinum doped (PMMA/ZrO2) and (PMMA/Al2O3) nanocomposites for electronics devices*, Transactions on Electrical and Electronic Materials, **21**, 550–563, 2020, https://doi.org/10.1007/s42341-020-00210-2.
7. R.Y. Hong, H.P. Fu, Y.J. Zhang, L. Liu, J. Wang, H.Z. Li, *Surface-modified silica nanoparticles for reinforcement of PMMA,* Journal of Applied Polymer Science, **105**, 2176–2184, 2007, https://doi.org/10.1002/app.26164.
8. G.R. Lashkaripour, R. Ajalloeian, *Determination of silica sand stiffness*, Engineering Geology, **68**, 225–236, 2003, https://doi.org/10.1016/S0013-7952(02)00229-6.
9. J. Thole, C. Beckermann, *Measurement of elastic modulus of PUNB bonded sand as a function of temperature*, International Journal of Metalcasting, **4**, 7–18, 2010, https://doi.org/10.1007/BF03355499.
10. Y. Lu, H. Wang, A.A. Luo, K. Ripplinger, *Process simulation and experimental validation of resin-bonded silica sand mold casting*, American Foundry Society Transactions, **125**, 215–220, 2017.

11. M.M. ISLAM, M.A. KABIR, H. KABIR, F. AHMED, M.A. GAFUR, *Physical, mechanical and thermal properties of sand reinforced polyester resin composite*, International Letters of Chemistry, Physics and Astronomy, **56**, 99–103, 2015, https://doi.org/0.18052/www.scipress.com/ILCPA.56.99.

12. H. BARGAOUI, F. AZZOUZ, D. THIBAULT, G. CAILLETAUD, *Thermomechanical behavior of resin bonded foundry sand cores during casting*, Journal of Materials Processing Technology, https://doi.org/10.1016/j.jmatprotec.2017.03.002.

13. G.R. CHATE, G.C.M. PATEL, R.M. KULKARNI, P. VERNEKAR, A.S. DESHPANDE, M.B. PARAPPAGOUDAR, *Study of the effect of nano-silica particles on resin-bonded moulding sand properties and quality of casting*, Silicon, **10**, 1921–1936, 2018, https://doi.org/10.1007/s12633-017-9705-z.

14. D. YEMAM, B.-J. KIM, J.-Y. MOON, C. YI, *Mechanical properties of epoxy resin mortar with sand washing waste as filler*, Materials, **10**, 246, 2017, https://doi.org/0.3390/ma10030246.

15. C.A. ANAGNOSTOPOULOS, T.T. PAPALIANGAS, *Experimental investigation of epoxy resin and sand mixes*, Journal of Geotechnical and Geoenvironmental Engineering, **138**, 841–9, 2012, https://doi.org/10.1061/(ASCE)GT.1943-5606.0000648.

16. E. OZEREN OZGUL, M.H. OZKUL, *Effects of epoxy, hardener, and diluent types on the workability of epoxy mixtures*, Construction and Building Materials, **158**, 369–77, 2018, https://doi.org/10.1016/j.conbuildmat.2017.10.008.

17. S.F.E. MATTUCCI, D.S. CRONIN, *A method to characterize average cervical spine ligament response based on raw data sets for implementation into injury biomechanics models*, Journal of the Mechanical Behaviour of Biomedical Materials, **41**, 251–60, 2015, https://doi.org/10.1016/j.jmbbm.2014.09.023.

18. R. WOLNY, T. WICZENBACH, A.J. ANDRZEJEWSKA, J.H. SPODNIK, *Mechanical response of human thoracic spine ligaments under quasi-static loading: An experimental study*, Journal of the Mechanical Behaviour of Biomedical Materials, **151**, 106404, 2024, https://doi.org/10.1016/j.jmbbm.2024.106404.

19. H.-J. WILKE, A. HERKOMMER, K. WERNER, C. LIEBSCH, *In vitro analysis of the segmental flexibility of the thoracic spine*, PLOS One, **12**, 5, e0177823, 2017, https://doi.org/10.1371/journal.pone.0177823.

20. J.J. COSTI, E.H. LEDET, G.D. O'CONNELL, *Spine biomechanical testing methodologies: The controversy of consensus vs scientific evidence*, JOR Spine 202, **4**, 1, 2021, https://doi.org/10.1002/jsp2.1138.

21. R. HIGUCHI, T. YOKOZEKI, K. NISHIDA, C. KAWAMURA, T. SUGIYAMA, T. MIYANAGA, *High-fidelity computational micromechanics of composite materials using image-based periodic representative volume element*, Composite Structures, **328**, 117726, 2024, https://doi.org/10.1016/j.compstruct.2023.117726.

22. J. QU, M. CHERKAOUI, *Fundamentals of Micromechanics of Solids*, Wiley, 2006, https://doi.org/10.1002/9780470117835.

23. V.A. BURYACHENKO, *Micromehcanics of Heterogenous Materials*, Springer, Boston, MA, 2007, https://doi.org/10.1007/978-0-387-68485-7.

24. S. YILMAZ, *An approach for predicting the elastic modulus of heterogeneous materials*, Materials and Design, **30**, 2938–45, 2009, https://doi.org/10.1016/j.matdes.2009.01.001.

25. K. Mazur, M. Krawczuk, L. Dąbrowski, *A new finite element with variable Young's modulus*, International Journal for Numerical Methods in Biomedical Engineering, **39**, 7, e3712, 2023, https://doi.org/10.1002/cnm.3712.

26. D. Gross, T. Seelig, *Fracture Mechanics*, Springer, Berlin, Heidelberg, 2011, https://doi.org/10.1007/978-3-642-19240-1.

27. J. Yvonnet, *Computational Homogenization of Heterogeneous Materials with Finite Elements*, **258**, Springer International Publishing, Cham, 2019, https://doi.org/10.1007/978-3-030-18383-7.

28. A. Sabik, M. Rucka, A. Andrzejewska, E. Wojtczak, *Tensile failure study of 3D printed 366 PLA using DIC technique and FEM analysis*, Mechanics of Materials, **175**, 104506, 2022, https://doi.org/10.1016/j.mechmat.2022.104506.

29. ASTM F2792–12, *Standard terminology for additive manufacturing technologies*, ASTM International, 2012.

30. Kulzer GmbH, *Kulzer Technik 2023*, https://kulzer-technik.com/en-kt/en-kt/home/homepage.html.

31. PN-EN 196-1:2016-07, *Metody badania cementu – Część 1: Oznaczanie wytrzymałości*, EN 196-1:2, Polski Komitet Normalizacyjny, 2016.

32. PN-EN 13395-1:2004. *Wyroby i systemy do ochrony i naprawy konstrukcji betonowych – Metody badań – Oznaczanie urabialności – Część 1: Badanie płynięcia zapraw tiksotropowych*, EN 13395-1, 2004.

33. P. Heyliger, H. Ledbetter, S. Kim, *Elastic constants of natural quartz*, Journal of the Acoustical Society of America, **114**, 644–50, 2003, https://doi.org/10.1121/1.1593063.

34. F.A. Pintar, N. Yoganandan, T. Myers, A. Elhagediab, A. Sances, *Biomechanical properties 380 of human lumbar spine ligaments,* Journal of Biomechanics, **25**, 11, 1351–6, 1992, https://doi.org/10.1016/0021-9290(92)90290-H.

35. N. Yoganandan, S. Kumaresan, F.A. Pintar, *Geometric and mechanical properties of human cervical spine ligaments*, Journal of Biomechanical Engineering, **122**, 623–9, 2000, https://doi.org/10.1115/1.1322034.

36. J. Chazal, A. Tanguy, M. Bourges, G. Gaurel, G. Escande, M. Guillot, G. Vanneuville, *Biomechanical properties of spinal ligaments and a histological study of the supraspinal ligament in traction*, Journal of Biomechanics, **18**, 167–76, 1985, https://doi.org/10.1016/0021-9290(85)90202-7.

37. L. Weng, Y. Shen, T. Fan, J. Xu, *A study of interface damage on mechanical properties of particle-reinforced composites*, Journal of The Minerals, Metals and Materials Society (JOM), **67**, 1499–504, 2015, https://doi.org/10.1007/s11837-015-1413-9.

Received September 18, 2024; revised version November 30, 2024.
Published online February 11, 2025.